

# On the $[\alpha/\text{Fe}]$ – $[\text{Fe}/\text{H}]$ relations in early-type galaxies

Fiorenzo Vincenzo<sup>1\*</sup>, Chiaki Kobayashi<sup>1</sup> & Philip Taylor<sup>2,3</sup>

<sup>1</sup>Centre for Astrophysics Research, University of Hertfordshire, College Lane, Hatfield, AL10 9AB, UK

<sup>2</sup>Research School of Astronomy and Astrophysics, Australian National University, Canberra, ACT 2611, Australia

<sup>3</sup>ARC Centre of Excellence for All Sky Astrophysics in 3 Dimensions (ASTRO 3D), Australia

Accepted 2018 July 7. Received 2018 June 22; in original form 2018 April 27

## ABSTRACT

We study how the predicted  $[\alpha/\text{Fe}]$ – $[\text{Fe}/\text{H}]$  relations in early-type galaxies vary as functions of their stellar masses, ages and stellar velocity dispersions, by making use of cosmological chemodynamical simulations with feedback from active galactic nuclei. Our model includes a detailed treatment for the chemical enrichment from dying stars, core-collapse supernovae (both Type II and hypernovae) and Type Ia supernovae. At redshift  $z = 0$ , we create a catalogue of 526 galaxies, among which we determine 80 early-type galaxies. From the analysis of our simulations, we find  $[\alpha/\text{Fe}]$ – $[\text{Fe}/\text{H}]$  relations similar to the Galactic bulge. We also find that, in the oldest galaxies, Type Ia supernovae start to contribute at higher  $[\text{Fe}/\text{H}]$  than in the youngest ones. On the average, early-type galaxies with larger stellar masses (and, equivalently, higher stellar velocity dispersions) have higher  $[\alpha/\text{Fe}]$  ratios, at fixed  $[\text{Fe}/\text{H}]$ . This is qualitatively consistent with the recent observations of Sybilka et al., but quantitatively there are mismatches, which might require stronger feedback, sub-classes of Type Ia Supernovae, or a variable initial mass function to address.

**Key words:** galaxies: abundances — galaxies: evolution — galaxies: elliptical and lenticular, cD — stars: abundances — hydrodynamics — supernovae: general

## 1 INTRODUCTION

The observed  $[\alpha/\text{Fe}]$  ratio historically represents one of the most used chemical diagnostics for Galactic and extragalactic astro-archaeology studies (e.g., Kobayashi 2016). The  $[\alpha/\text{Fe}]$ – $[\text{Fe}/\text{H}]$  chemical abundance pattern was initially shown for the solar neighborhood and has been used to understand the origin of Type Ia Supernovae (SNe Ia) (e.g., Matteucci & Greggio 1986; Kobayashi et al. 1998). Later, the observed  $[\alpha/\text{Fe}]$  ratios in nearby elliptical galaxies were used to constrain their formation scenario (Matteucci 1994; Thomas et al. 2010). Although various types of models have been suggested (Pipino & Matteucci 2004; Kobayashi 2004; De Lucia et al. 2006; Taylor & Kobayashi 2015; De Lucia et al. 2017; De Masi et al. 2018), the observed correlations between  $[\alpha/\text{Fe}]$  and other physical and chemical properties of early-type galaxies (ETGs) still represent unsolved problems for galaxy formation and evolution in a cosmological context.

In our Milky Way (MW), the  $[\alpha/\text{Fe}]$ – $[\text{Fe}/\text{H}]$  abundance ratio pattern (which can be separately measured in the halo, bulge, thick and thin disc stellar components) can be effectively used to probe the characteristic star formation histories (SFHs) of the different MW stellar components (e.g., Matteucci 2012). The specific trend of  $[\alpha/\text{Fe}]$  versus  $[\text{Fe}/\text{H}]$  in our Galaxy (Kobayashi et al. 2011) and the similar trends in its dwarf spheroidal galaxy satellites (Lanfranchi &

Matteucci 2004) can be explained as the consequence of the different channels for the nucleosynthesis of  $\alpha$ -elements (O, Mg, Ne, Si, S, and Ca) and iron. On the one hand,  $\alpha$ -elements are mainly produced on short timescales ( $\sim 10^6$  yr) by core-collapse supernovae (SNe), which can also eject some iron into the interstellar medium (ISM) of galaxies; in particular, core-collapse SNe represent the only source of Fe in the earliest stages of the galaxy evolution. On the other hand, the bulk of iron is produced by SNe Ia on longer timescales, causing  $[\alpha/\text{Fe}]$  to decrease. SN Ia progenitors are not well understood yet, and there may be multiple channels, but – in any case – the timescale is at least  $\sim 0.01$  Gyr (e.g., Kobayashi & Nomoto 2009).

In elliptical galaxies,  $[\alpha/\text{Fe}]$  and  $[\text{Fe}/\text{H}]$  can be estimated from absorption lines (e.g., Faber 1973; Worthey et al. 1994; Thomas & Maraston 2003; Cervantes & Vazdekis 2009), and the correlations with a variety of different galaxy properties such as stellar mass, age, and environments have been shown (e.g., Thomas et al. 2010; Kuntschner et al. 2010; Spolaor et al. 2010). Recently, Kriek et al. (2016) showed very high  $[\alpha/\text{Fe}]$  ratios in ETGs at redshift  $z = 2$ ; this observation made it harder to explain the formation of massive galaxies in a cosmological context. Moreover, with integral-field unit (IFU) observations of nearby ETGs, Sybilka et al. (2018) showed a mass-dependence of the  $[\text{Mg}/\text{Fe}]$ – $[\text{Fe}/\text{H}]$  relation. In this Letter, using our cosmological chemodynamical simulations that include feedback from active galactic nuclei (AGN) and a detailed treatment for the chemical enrichment, we aim to understand the observational result in Sybilka et al. (2018).

\* f.vincenzo@herts.ac.uk

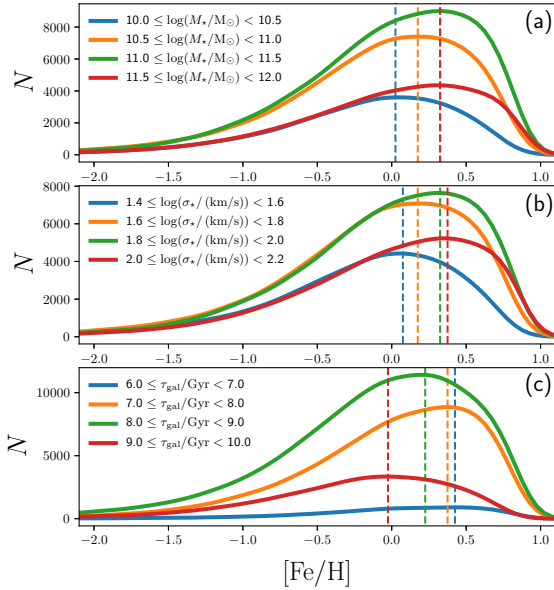


**Figure 1.** The  $[\text{Fe}/\text{H}]$  distribution function of all the stellar populations in our simulated ETGs within a given stellar mass bin (panel a), stellar velocity dispersion bin (panel b) and galaxy age bin (panel c). The vertical dashed lines correspond to the  $[\text{Fe}/\text{H}]$  abundances at the maximum of each distribution.

This Letter is structured as follows. In Section 2, we describe our cosmological chemodynamical simulation and the methods of analysis. In Section 3, we present our results, mostly focusing on how the predicted  $[\alpha/\text{Fe}]$ – $[\text{Fe}/\text{H}]$  relations in ETGs vary as functions of their stellar mass and age. In Section 4, we draw our conclusions.

## 2 MODEL, SIMULATIONS AND METHODS

### 2.1 The model

We analyse two cosmological simulations run by our chemodynamical code based on GADGET-3, a smoothed-particle hydrodynamics code (Springel 2005). Our code has been developed by Kobayashi (2004); Kobayashi et al. (2007); Taylor & Kobayashi (2014) to include the relevant baryon physical processes such as UV background heating; metal-dependent radiative cooling; star formation activity with the corresponding thermal energetic feedback from stellar winds and SN explosions; formation of black hole (BH) seeds as the debris of the first stars; the growth and feedback from AGN; finally, chemical enrichment from AGB stars and core-collapse SNE and SNe Ia. The thermal energetic feedback and the nucleosynthetic products are distributed, kernel-weighted, to a fixed number of neighbour gas particles,  $N_{\text{FB}} = 72$ .

We adopt the mass and metallicity-dependent stellar yields of Kobayashi et al. (2011) and the metallicity-dependent stellar lifetimes as in Kobayashi et al. (2007). Finally, we assume the universal Kroupa (2008) initial mass function (IMF), defined in the mass range  $0.01 \leq m \leq 120 M_{\odot}$ .

*SN Ia model* — For the predictions of  $[\alpha/\text{Fe}]$  ratios, the most important factor is the SN Ia model. Our model is based on Chandrasekhar mass explosions of C+O white dwarfs (WDs) in single-degenerate systems. Because of the WD winds, our SN Ia rate depends on the metallicity, and becomes zero below the progenitor  $[\text{Fe}/\text{H}] = -1.1$  (Kobayashi et al. 1998). This model gives an excel-

lent agreement with the observed  $[\alpha/\text{Fe}]$  and  $[\text{Mn}/\text{Fe}]$  in the solar neighbourhood. The shortest lifetime is 0.5 Gyr at  $[\text{Fe}/\text{H}] = -1.0$ , and becomes 0.1 Gyr at  $[\text{Fe}/\text{H}] = 0.0$  (see Kobayashi & Nomoto 2009, for the details). In nearby galaxies, the lifetime distribution is very similar to the observed delay-time distribution of nearby SNe Ia, and also to that of a simple model of double degenerate systems (Maoz, Mannucci & Nelemans 2014). Note that sub-classes of SNe Ia (Kobayashi et al. 2015) are not included (see also Section 3.3).

*AGN feedback* — In order to model massive ETGs, it is necessary to include additional feedback, and the feedback from AGN is the most likely as it can work in a deep potential well. The co-evolution between AGN and galaxy stellar components is supported from the observed BH mass–bulge mass relation (e.g., Magorrian et al. 1998). Our AGN model successfully reproduces a number of observed properties of galaxies, including the cosmic SFRs (Taylor & Kobayashi 2014), galaxy size–mass relations, mass–metallicity relations (MZR; Taylor & Kobayashi 2015, 2016), and metallicity radial gradients (Taylor & Kobayashi 2017). Here we briefly recall that BHs are assumed to form from metal-free gas with volume mass density above  $\rho_c = 0.1 h^2 m_{\text{H}} \text{cm}^{-3}$ . The initial seed mass of the primordial BHs is  $M_{\text{BH,seed}} = 1000 h^{-1} M_{\odot}$ ; then, the BH mass can grow as a function of time via Eddington-limited, Bondi-Hoyle gas accretion. The mass growth of the BHs is due to gas accretion from the surrounding ISM and mergers with other BHs, which – in turn – trigger the AGN activity. The AGN rate of thermal energy feedback is directly proportional to the accretion rate onto the BH.

### 2.2 The simulations

We use two simulations of a cubic volume for the standard  $\Lambda$ -cold dark matter Universe, with periodic boundary conditions and cosmological parameters from the nine-year Wilkinson Microwave Anisotropy Probe (Hinshaw et al. 2013,  $\Omega_0 = 0.28$ ,  $\Omega_{\Lambda} = 0.72$ ,  $\Omega_b = 0.046$ ,  $H_0 = 100 \times h = 70 \text{ km s}^{-1} \text{ Mpc}$ , and  $\sigma_8 = 0.82$ ).

Simulation A is the same simulation as used in Taylor & Kobayashi (2016), with an initial condition giving rise to a strong central concentration of galaxies at redshift  $z = 0$ . This simulation has a volume of  $(25 \text{ Mpc } h^{-1})^3$  and total number of dark matter (DM) and gas particles  $N_{\text{DM}} = N_{\text{gas}} = (240)^3$ . The mass resolutions are  $M_{\text{gas}} = 1.44 \times 10^7 h^{-1} M_{\odot}$  and  $M_{\text{DM}} = 7.34 \times 10^7 h^{-1} M_{\odot}$  for the gas and DM particles, respectively; the gravitational softening length of gas is  $\epsilon_g = 1.125 \text{ kpc } h^{-1}$ .

Simulation B corresponds to the  $\Theta 10\text{Mpc}128$  simulation in Taylor & Kobayashi (2014), but with the same initial condition as in Kobayashi et al. (2007). This shows a weak concentration of galaxies in the box at redshift  $z = 0$ , which corresponds to the field environment. This simulation has a volume of  $(10 \text{ Mpc } h^{-1})^3$  and  $N_{\text{DM}} = N_{\text{gas}} = (128)^3$ . The mass resolutions are  $M_{\text{gas}} = 6.09 \times 10^6 h^{-1} M_{\odot}$  and  $M_{\text{DM}} = 3.10 \times 10^7 h^{-1} M_{\odot}$ , with  $\epsilon_g = 0.844 \text{ kpc } h^{-1}$ .

Each star particle in the simulation corresponds to a simple stellar population with fixed age and metallicity; the typical masses of the star particles are in the range between  $3\text{--}7 \times 10^6 h^{-1} M_{\odot}$  (see Kobayashi et al. 2007 for the detailed model of star formation). In this Letter, the star particles within a given simulated galaxy are called “stellar populations”.

### 2.3 Methods

We adopt the code ROCKSTAR (Behroozi et al. 2013), to create a catalogue of DM haloes from simulations A and B at redshift  $z = 0$ . Due

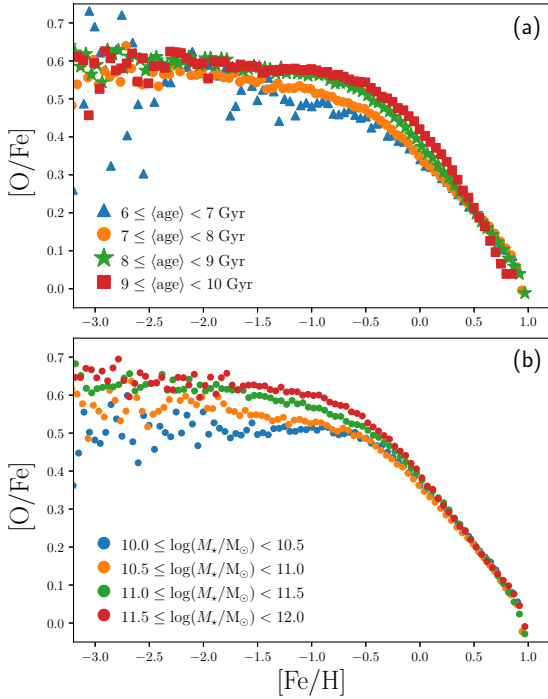


**Figure 2.** The  $[\text{O}/\text{Fe}]$ – $[\text{Fe}/\text{H}]$  chemical evolution tracks of all our simulated ETGs as functions of the average galaxy stellar age (panel a) and total galaxy stellar mass (panel b).

to the limited resolutions of our simulations, we only include in the catalogue the DM haloes with virial masses  $M_{\text{vir,DM}} \geq 10^{11} M_\odot$ .

We isolate and analyse 486 galaxies and 40 galaxies in the simulations A and B, respectively. In total, we have 526 galaxies in our catalogue, with total stellar mass  $9.0 \lesssim \log(M_\star/M_\odot) \lesssim 11.8$ . This covers the mass range of the observations.

In the catalogue, each galaxy is defined by considering all the gas and star particles within the scale radius of a Navarro-Frenk-White profile fitted to the dark matter halo. For each galaxy, we visually check that our automated algorithm properly works in selecting and isolating all the star and gas particles within the scale radius of the host DM halo, in order to exclude any external contributions from close satellites or merging companions.

ETGs are determined from the same criterion of Fossati et al. (2015) (see also Spitoni et al. 2017 and Taylor & Kobayashi 2017); namely, one galaxy is defined as “passive” if its specific star formation rate (SFR)  $s\text{SFR} = \text{SFR}/M_\star < b/t_{z0} \approx 2.17 \times 10^{-11} \text{ yr}^{-1}$ , where  $b = \text{SFR}/\langle \text{SFR} \rangle = 0.3$  is the so-called birthrate parameter (Sandage 1986; Franx et al. 2008) and  $t_{z0}$  is the age of the Universe at redshift  $z = 0$ . Eventually we have 80 ETGs in our catalogue, 61 from simulation A and 19 from simulation B. There is no significant difference in the SFRs and MZR between simulations A and B (Kacprzak et al. 2015), although massive galaxies are found only in simulation A.

In order to compare with the observed mass-dependence of the  $[\text{Mg}/\text{Fe}]$ – $[\text{Fe}/\text{H}]$  relations in ETGs, we applied the following scheme of our analysis, similar to that in Sybilaska et al. (2018).

(i) For each ETG in the catalogue, we compute  $[\text{Fe}/\text{H}]$  and  $[\text{O}/\text{Fe}]$  of all its stellar populations. We assume the Asplund et al. (2009) solar abundances.

(ii) The ETGs are divided into bins of either  $\log(M_\star/M_\odot)$ , average stellar age, or average stellar velocity dispersion. We use bins of

width  $\Delta \log(M_\star/M_\odot) = 0.5$ ,  $\Delta \tau = 1$  Gyr, and  $\Delta \log(\sigma/(\text{km s}^{-1})) = 0.2$ , respectively.

(iii) For each bin of  $\log(M_\star/M_\odot)$ , age or  $\log(\sigma/(\text{km s}^{-1}))$ , all the galaxy stellar populations of (1) are binned according to their  $[\text{Fe}/\text{H}]$  abundance, by assuming a bin width  $\Delta[\text{Fe}/\text{H}] = 0.05$ ; within each  $[\text{Fe}/\text{H}]$  bin, we compute the average  $[\text{O}/\text{Fe}]$  ratio. There is no significant change if we weight by mass or luminosity.

### 3 RESULTS

In Figure 1(a), we show how the iron abundance distribution function of all the stellar populations in our simulated ETGs is predicted to vary as a function of the total galaxy stellar mass; different colours in the figure correspond to galaxies lying in different bins of  $\log(M_\star/M_\odot)$ . We find that ETGs with increasing stellar mass have the distribution peaked towards higher and higher  $[\text{Fe}/\text{H}]$ .

Since there is a straight correlation between the total galaxy stellar mass and the stellar velocity dispersion,  $\sigma$ , we also find that galaxies with larger values of  $\sigma$  have stellar populations with higher  $[\text{Fe}/\text{H}]$ , on average (Figure 1(b)). In Figure 1(c), we show the  $[\text{Fe}/\text{H}]$ -distribution for different bins of galaxy age, where the peak is at lower  $[\text{Fe}/\text{H}]$  for older stellar populations. Note that most of the ETGs in our sample have ages  $7 \leq \tau_{\text{gal}} < 9$  Gyr and that there are very few ETGs which have ages  $6 \leq \tau_{\text{gal}} < 7$  Gyr and  $[\text{Fe}/\text{H}] \lesssim -1.0$ .

#### 3.1 The age-dependence

In Figure 2(a), we study the age-dependence of the  $[\text{O}/\text{Fe}]$ – $[\text{Fe}/\text{H}]$  relations in our sample of ETGs; different colours in the figure correspond to different average stellar ages of the galaxies.  $[\text{O}/\text{Fe}]$  ratios are, on average, almost constant at  $[\text{Fe}/\text{H}] \lesssim -2$ , independent of stellar age. Then, we find that ETGs with older ages have higher average  $[\text{O}/\text{Fe}]$  at fixed  $[\text{Fe}/\text{H}]$ . Finally, such a difference between chemical evolution tracks with different age steadily diminishes with increasing  $[\text{Fe}/\text{H}]$ .

To understand the predicted behaviour of  $[\text{O}/\text{Fe}]$  versus  $[\text{Fe}/\text{H}]$ , we recall that at very low  $[\text{Fe}/\text{H}]$ , the  $[\text{O}/\text{Fe}]$  ratios mostly reflect the chemical enrichment from core-collapse SNe, which produce both O and Fe on a short timescale after the star formation event. The IMF-weighted core-collapse SN yields determine a so-called “plateau” in the chemical evolution tracks. Then, as we move towards higher and higher  $[\text{Fe}/\text{H}]$ , the models predict a knee in the  $[\text{O}/\text{Fe}]$ – $[\text{Fe}/\text{H}]$  diagram, which is due to the larger amounts of Fe that SNe Ia inject in the galaxy ISM on a longer timescale. In Figure 2(a), the position of this knee in the  $[\text{O}/\text{Fe}]$ – $[\text{Fe}/\text{H}]$  diagram turns out to depend on the galaxy stellar age.

ETGs with SFH peaked at very high redshift have the knee in the  $[\text{O}/\text{Fe}]$ – $[\text{Fe}/\text{H}]$  diagram at higher  $[\text{Fe}/\text{H}]$  than young ETGs. This means that, in such oldest galaxies, when SNe Ia start to contribute, the  $[\text{Fe}/\text{H}]$  of the ISM is already very high; this can only happen (i) if the SFR in the oldest galaxies is more intense and more temporally concentrated than in the youngest ETGs, and (ii) if the chemical enrichment efficiency in the oldest ETGs is higher than in the youngest ones (or, equivalently, if the chemical enrichment timescales are shorter). Note that, although short star formation timescales can be inferred from the observed stellar ages or  $[\alpha/\text{Fe}]$  ratios, short chemical enrichment timescales can be clearly confirmed with the  $[\alpha/\text{Fe}]$ – $[\text{Fe}/\text{H}]$  relations. Even with rapid star formation, the evolutionary tracks of  $[\alpha/\text{Fe}]$ – $[\text{Fe}/\text{H}]$  cannot be described with the so-called “closed-box model” (where the gas

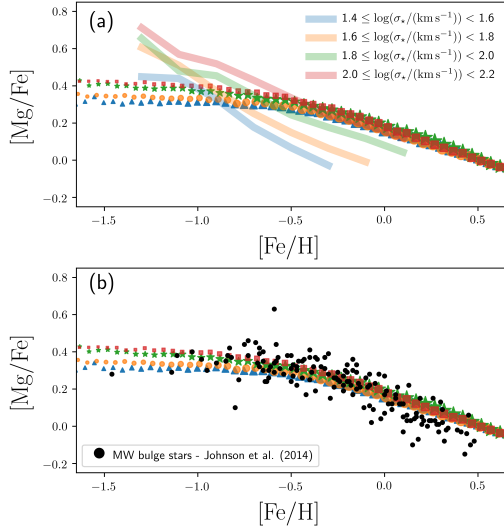


**Figure 3.** The  $[\text{Mg}/\text{Fe}]$ – $[\text{Fe}/\text{H}]$  chemical evolution tracks. In panel (a), the solid curves represent the observed data of Sybilka et al. (2018) and the points represent our model predictions, where different colours correspond to different stellar velocity dispersions of the galaxies. In panel (b), the black points represent the abundance measurements in the MW bulge stars from Johnson et al. (2014).

fraction is already high when the galaxy formed), but only with the so-called “infall model”, where the initial gas fraction is small and the star formation is directly driven by the gas infall (Tinsley 1980; Kobayashi et al. 2000). The loss of metals by SN- and AGN-driven outflows does not appear at early stages in this figure, which is reasonable because of the deep potential well of the majority of galaxies and of the co-evolution of the AGN and its host galaxy.

The difference in the chemical evolution tracks becomes smaller with increasing  $[\text{Fe}/\text{H}]$ . This is a signature of the fact that the chemical enrichment from SNe Ia dominates at high  $[\text{Fe}/\text{H}]$  over all the other nucleosynthetic processes, causing the ISM to saturate towards a common level of  $[\alpha/\text{Fe}]$  ratios for all galaxies, despite their average stellar age.

Our final consideration on Figure 2(a) is about the large scatter in the predicted  $[\text{O}/\text{Fe}]$  ratios at very low  $[\text{Fe}/\text{H}]$ , for ETGs with ages in the range  $6 \leq \tau_{\text{gal}} < 7 \text{ Gyr}$ ; this is due to the very low number of stellar populations with very low  $[\text{Fe}/\text{H}]$  within this age bin (see also Figure 1c).  $[\text{O}/\text{Fe}]$  ratios of such stars reflect the variation in the yields of individual core-collapse SNe; more massive ( $\sim 40 M_{\odot}$ ) SNe give higher  $[\text{O}/\text{Fe}]$  than low-mass ( $\sim 15 M_{\odot}$ ) SNe (Kobayashi et al. 2006). This effect is included in the inhomogeneous enrichment in our chemodynamical code (see Kobayashi & Nakasato 2011, for more details).

### 3.2 The mass-dependence

In Figure 2(b), we study the mass-dependence of the  $[\text{O}/\text{Fe}]$ – $[\text{Fe}/\text{H}]$  relation for the same sample of galaxies as in Figure 2(a). In Taylor & Kobayashi (2015, their figure 10), which used the same simulation as in this Letter, it was shown that more massive ETGs are also older, on average. Nevertheless, the age-mass relation is not perfect especially for less-massive/young ETGs; for this reason, we find a different dependence of  $[\text{O}/\text{Fe}]$ – $[\text{Fe}/\text{H}]$  as a function of the galaxy stellar mass. In particular, we predict  $[\text{O}/\text{Fe}]$  plateau values which are smaller for less massive ETGs, on average.

The  $[\text{O}/\text{Fe}]$  plateau value depends on the relative contribution between core-collapse and SNe Ia, before SNe Ia become predominant. In less-massive ETGs, it took longer to reach  $[\text{Fe}/\text{H}] = -1$  because of the lower SFRs, and young stars can form from low-metallicity ISM already enriched by SNe Ia; in massive ETGs, there is not so much low-metallicity ISM. In addition, a part of the early chemical enrichment from core-collapse SNe might be lost through SN-driven outflows in the shallower potential wells of less-massive systems. Finally, the variation in  $[\text{O}/\text{Fe}]$  at very low  $[\text{Fe}/\text{H}]$  is the consequence of an inhomogeneous chemical enrichment (Vincenzo & Kobayashi 2018), which is particularly important for low-mass galaxies. This is one of the main features of chemodynamical simulations (Kobayashi & Nakasato 2011), which cannot be obtained by classical one- or multi-zone chemical evolution models.

### 3.3 Comparing the model with observations

The observed data set is taken from Sybilka et al. (2018), which provide  $[\text{Mg}/\text{Fe}]$ , metallicity, and stellar velocity dispersions for a sample of 258 ETGs in the ATLAS<sup>3D</sup> project (Cappellari et al. 2011); we remark on the fact that most of these galaxies are spatially resolved, thanks to the SAURON integral field unit (IFU) instrument at the William Herschel Telescope; 58 galaxies in the sample of Sybilka et al. (2018) lie in the Virgo cluster, and the remaining 200 galaxies lie in the field/group environment.

It is important to note that the iron abundances in Sybilka et al. (2018) have been estimated with the following empirical formula:  $[\text{Fe}/\text{H}] = [\text{Z}/\text{H}] - 0.75 \times [\text{Mg}/\text{Fe}]$  (Vazdekis et al. 2015), where  $[\text{Z}/\text{H}]$  represents the abundance of all metals. This might cause an uncertainty in the derivation of chemical abundances.

In our simulation, we did not follow Mg, and we use O as a representative of  $\alpha$ -elements. All  $\alpha$ -elements follow a very similar  $[\alpha/\text{Fe}]$ – $[\text{Fe}/\text{H}]$  relations as O shows. In the adopted nucleosynthesis yields,  $[\text{O}/\text{Mg}]$  is almost zero, independent of metallicity, which was consistent with local thermodynamic equilibrium (LTE) observations of stars in the solar neighbourhood (Kobayashi et al. 2006). However, recent non-LTE observations suggested  $[\text{O}/\text{Mg}] \sim 0.2$  at a wide range of metallicity (Zhao et al. 2016). Therefore, for the comparison to the galaxy observation, we apply a correction of  $-0.2$  to the predicted  $[\text{O}/\text{Fe}]$  ratios of our simulation.

In Figure 3(a), we compare our predicted  $[\text{Mg}/\text{Fe}]$ – $[\text{Fe}/\text{H}]$  relations (points with different colours) with the observations (solid curves); in the figure, different colours correspond to different bins of stellar velocity dispersion,  $\sigma$ . The observations show parallel trends of  $[\text{Mg}/\text{Fe}]$  against  $[\text{Fe}/\text{H}]$ , where more massive ETGs have higher  $[\text{Mg}/\text{Fe}]$  at fixed  $[\text{Fe}/\text{H}]$ . Our cosmological chemodynamical simulations reproduce the slope of  $[\text{Mg}/\text{Fe}]$  at  $[\text{Fe}/\text{H}] \gtrsim -0.5$  of massive galaxies very well. We also see a similar mass-dependence of the  $[\text{Mg}/\text{Fe}]$ – $[\text{Fe}/\text{H}]$  relations. However, our correlation is weaker than in the observations. At  $[\text{Fe}/\text{H}] \lesssim -0.5$ , our slope of  $[\text{Mg}/\text{Fe}]$  versus  $[\text{Fe}/\text{H}]$  is shallower than in the observations. We also note that the majority of our massive ETGs are dominated by metal-rich stellar populations (Fig. 1), while most of the galaxies in the Sybilka et al. (2018) sample show sub-solar metallicities. This is already seen in the predicted MZR, where our simulated galaxies are in good agreement with other observations, but show higher metallicities than in ATLAS<sup>3D</sup> (Taylor & Kobayashi 2016).

The observed trend for the least massive ETGs could be reproduced, for example, by assuming stronger SN and/or AGN feedback associated with metal loss in less-massive systems. Alternatively, additional sub-classes of SNe Ia such as sub-Chandrasekhar SNe Ia or the so-called SNe Iax could produce a sharp  $[\alpha/\text{Fe}]$  decrease

at lower  $[\text{Fe}/\text{H}]$  (Kobayashi et al. 2015); finally, the observed data might suggest a variable IMF, which – in turn – would affect our net yields of metals; in particular, a bottom-heavy IMF would give low  $[\alpha/\text{Fe}]$ . If the IMF is more bottom-heavy for low-mass galaxies, that might explain the observations (see also Kobayashi 2010; De Masi et al. 2018), however, this is the opposite from what is suggested by other observations such as Cenarro et al. (2003); Parikh et al. (2018).

Our final consideration on Figure 3(a) is that there might be an uncertainty in the calibration of observations; moreover, the absence of a plateau in the observed data might be due intrinsic uncertainties in the IFU observations, because low  $[\text{Fe}/\text{H}]$  abundances are observed in the outer galaxy regions, where the surface brightness becomes fainter.

In Figure 3(b), the  $[\text{Mg}/\text{Fe}]$ – $[\text{Fe}/\text{H}]$  relations in our simulated ETGs are compared with the observed chemical abundance measurements in the MW stellar bulge by Johnson et al. (2014). We find that the chemical evolution tracks in our simulated ETGs are qualitatively in agreement with the observations in the Galactic bulge. We notice that the decreasing trend of  $[\text{Mg}/\text{Fe}]$ – $[\text{Fe}/\text{H}]$  is more similar to the observations of Sybilka et al. (2018) for ETGs with  $1.8 \leq \log(\sigma_*/(\text{km/s})) \leq 2.2$ , which is consistent with the average stellar velocity dispersions in the Galactic bulge (Johnson et al. 2014).

#### 4 CONCLUSIONS

We studied how the average  $[\alpha/\text{Fe}]$ – $[\text{Fe}/\text{H}]$  relations in a catalogue of simulated ETGs correlate with the galaxy stellar mass and age. We also compared the predictions of our cosmological chemodynamical simulations with AGN feedback with the latest observational results of Sybilka et al. (2018). Our main conclusions can be summarised as follows.

(i) At low  $[\text{Fe}/\text{H}]$ , we predict an  $[\alpha/\text{Fe}]$  plateau, with higher values for more massive galaxies. The position of the knee in  $[\alpha/\text{Fe}]$ – $[\text{Fe}/\text{H}]$  is determined both by the galaxy SFH and by the chemical enrichment timescale, and it is more sensitive to the average galaxy stellar age than mass.

(ii) Our simulations can qualitatively explain the observed mass-dependence of  $[\text{Mg}/\text{Fe}]$ – $[\text{Fe}/\text{H}]$ , but quantitatively there are mismatches. In particular, less massive ETGs in the observations show even earlier decrease in  $[\text{Mg}/\text{Fe}]$  than in our model. This suggests even lower chemical enrichment efficiencies in low-mass ETGs than in our model.

(iii) There might be an uncertainty in the calibration of observations, our net yields might be too high, stronger AGN/SN feedback or additional classes of SNe Ia might be required. Also an IMF which is more bottom-heavy for less-massive systems might help to reproduce the observational data.

#### ACKNOWLEDGMENTS

We thank an anonymous referee for many comments and suggestions. We thank V. Springel for providing GADGET-3, A. Sybilka and H. Kuntschner for providing the observational data. FV and CK acknowledge funding from STFC (ST/M000958/1). PT acknowledges funding through a Discovery Projects grant from the Australian Research Council (grant no. DP150104329). This work used the DiRAC Data Centric system (part of the National E-Infrastructure), funded by Durham University and grants ST/K00042X/1, ST/K00087X/1 & ST/K003267/1.

#### References

- Asplund, M., Grevesse, N., Sauval, A. J., & Scott, P. 2009, *ARA&A*, 47, 481
- Behroozi P. S., Wechsler R. H., Wu, H.-Y. 2013, *ApJ*, 762, 109
- Cappellari, M., Emsellem, E., Krajnović, D., et al. 2011, *MNRAS*, 413, 813
- Cenarro, A. J., Gorgas, J., Vazdekis, A., Cardiel, N., & Peletier, R. F. 2003, *MNRAS*, 339, L12
- Cervantes, J. L., & Vazdekis, A. 2009, *MNRAS*, 392, 691
- De Lucia, G., Springel, V., White, S. D. M., Croton, D., & Kauffmann, G. 2006, *MNRAS*, 366, 499
- De Lucia, G., Fontanot, F., & Hirschmann, M. 2017, *MNRAS*, 466, L88
- De Masi, C., Matteucci, F., & Vincenzo, F. 2018, *MNRAS*, 474, 5259
- Faber, S. M. 1973, *ApJ*, 179, 731
- Fossati, M., Wilman, D. J., Fontanot, F., et al. 2015, *MNRAS*, 446, 2582
- Franx, M., van Dokkum, P. G., Förster Schreiber, N. M., et al. 2008, *ApJ*, 688, 770–788
- Hinshaw G., Larson D., Komatsu E., et al., 2013, *ApJS*, 208, 19
- Johnson C. I., Rich R. M., Kobayashi C., Kunder A., Koch A., 2014, *AJ*, 148, 67
- Lanfranchi, G. A., & Matteucci, F. 2004, *MNRAS*, 351, 1338
- Magorrian, J. et al. 1998, *ApJ*, 115, 2285
- Maoz, D., Mannucci, F., & Nelemans, G. 2014, *ARA&A*, 52, 107
- Matteucci, F., & Greggio, L. 1986, *A&A*, 154, 279
- Matteucci, F. 1994, *A&A*, 288, 57
- Matteucci F. 2012, Springer-Verlag, Berlin, Heidelberg
- Parikh, T., Thomas, D., Maraston, C., et al. 2018, *MNRAS*,
- Pipino, A., & Matteucci, F. 2004, *MNRAS*, 347, 968
- Sandage, A. 1986, *A&A*, 161, 89
- Spitoni, E., Vincenzo, F., & Matteucci, F. 2017, *A&A*, 599, A6
- Springel V., 2005, *MNRAS*, 364, 1105
- Sybilka, A., Kuntschner, H., van de Ven, G., et al. 2018, *MNRAS*, 476, 4501
- Kacprzak, G. G., Yuan, T., Nanayakkara, T., et al. 2015, *ApJ*, 802, L26
- Kobayashi, C., Tsujimoto, T., Nomoto, K., Hachisu, I., & Kato, M. 1998, *ApJ*, 503, L155
- Kobayashi, C., Tsujimoto, T., & Nomoto, K. 2000, *ApJ*, 539, 26
- Kobayashi C., 2004, *MNRAS*, 347, 740
- Kobayashi, C., Umeda, H., Nomoto, K., Tominaga, N., & Ohkubo, T. 2006, *ApJ*, 653, 1145
- Kobayashi C., Springel V., White S. D. M., 2007, *MNRAS*, 376, 1465
- Kobayashi, C., & Nomoto, K. 2009, *ApJ*, 707, 1466
- Kobayashi, C. 2010, *American Institute of Physics Conference Series*, 1240, 123
- Kobayashi C., Nakasato N., 2011, *ApJ*, 729, 16
- Kobayashi C., Karakas A. I., Umeda H., 2011, *MNRAS*, 414, 3231
- Kobayashi, C., Nomoto, K., & Hachisu, I. 2015, *ApJ*, 804, L24
- Kobayashi, C. 2016, *Nature*, 540, 205
- Kriek, M., Conroy, C., van Dokkum, P. G., et al. 2016, *Nature*, 540, 248
- Kroupa, P., 2008, *Pathways Through an Eclectic Universe*, 390, 3
- Kuntschner, H., Emsellem, E., Bacon, R., et al. 2010, *MNRAS*, 408, 97
- Spolaor, M., Kobayashi, C., Forbes, D. A., Couch, W. J., & Hau, G. K., 2009, *MNRAS*, 408, 272
- Taylor, P., & Kobayashi, C. 2014, *MNRAS*, 442, 2751
- Taylor, P., & Kobayashi, C. 2015, *MNRAS*, 448, 1835
- Taylor, P., & Kobayashi, C. 2016, *MNRAS*, 463, 2465
- Taylor, P., & Kobayashi, C. 2017, *MNRAS*, 471, 3856
- Thomas, D., & Maraston, C. 2003, *A&A*, 401, 429
- Thomas, D., Maraston, C., Schawinski, K., Sarzi, M., & Silk, J. 2010, *MNRAS*, 404, 1775
- Tinsley, B. M. 1980, *Fundamentals Cosmic Phys.*, 5, 287
- Vazdekis, A., Coelho, P., Cassisi, S., et al. 2015, *MNRAS*, 449, 1177
- Vincenzo, F., & Kobayashi, C. 2018, *A&A*, 610, L16
- Worthey, G., Faber, S. M., Gonzalez, J. J., & Burstein, D. 1994, *ApJS*, 94, 687
- Zhao, G., Mashonkina, L., Yan, H. L., Alexeeva, S., Kobayashi, C., et al. 2016, *ApJ*, 833, 225